
Learning to Transduce with Unbounded Memory

Edward Grefenstette
Google DeepMind
etg@google.com

Karl Moritz Hermann
Google DeepMind
kmh@google.com

Mustafa Suleyman
Google DeepMind
mustafasul@google.com

Phil Blunsom
Google DeepMind and Oxford University
pblunsom@google.com

Abstract

Recently, strong results have been demonstrated by Deep Recurrent Neural Networks on natural language transduction problems. In this paper we explore the representational power of these models using synthetic grammars designed to exhibit phenomena similar to those found in real transduction problems such as machine translation. These experiments lead us to propose new memory-based recurrent networks that implement continuously differentiable analogues of traditional data structures such as Stacks, Queues, and DeQues. We show that these architectures exhibit superior generalisation performance to Deep RNNs and are often able to learn the underlying generating algorithms in our transduction experiments.

1 Introduction

Recurrent neural networks (RNNs) offer a compelling tool for processing natural language input in a straightforward sequential manner. Many natural language processing (NLP) tasks can be viewed as transduction problems, that is learning to convert one string into another. Machine translation is a prototypical example of transduction and recent results indicate that Deep RNNs have the ability to encode long source strings and produce coherent translations [1, 2]. While elegant, the application of RNNs to transduction tasks requires hidden layers large enough to store representations of the longest strings likely to be encountered, implying wastage on shorter strings and a strong dependency between the number of parameters in the model and its memory.

In this paper we use a number of linguistically-inspired synthetic transduction tasks to explore the ability of RNNs to learn long-range reorderings and substitutions. Further, inspired by prior work on neural network implementations of stack data structures [3], we propose and evaluate transduction models based on Neural Stacks, Queues, and DeQues (double ended queues). Stack algorithms are well-suited to processing the hierarchical structures observed in natural language and we hypothesise that their neural analogues will provide an effective and learnable transduction tool. Our models provide a middle ground between simple RNNs and the recently proposed Neural Turing Machine (NTM) [4] which implements a powerful random access memory with read and write operations. Neural Stacks, Queues, and DeQues also provide a logically unbounded memory while permitting efficient constant time push and pop operations.

Our results indicate that the models proposed in this work, and in particular the Neural DeQue, are able to consistently learn a range of challenging transductions. While Deep RNNs based on long

This version of the paper is identical to the version found in the proceedings of *Advances in Neural Information Processing Systems*, 2015, with the addition of some missing references. Figures have been made larger for increased legibility.

short-term memory (LSTM) cells [1, 5] can learn some transductions when tested on inputs of the same length as seen in training, they fail to consistently generalise to longer strings. In contrast, our sequential memory-based algorithms are able to learn to reproduce the generating transduction algorithms, often generalising perfectly to inputs well beyond those encountered in training.

2 Related Work

String transduction is central to many applications in NLP, from name transliteration and spelling correction, to inflectional morphology and machine translation. The most common approach leverages symbolic finite state transducers [6, 7], with approaches based on context free representations also being popular [8]. RNNs offer an attractive alternative to symbolic transducers due to their simple algorithms and expressive representations [9]. However, as we show in this work, such models are limited in their ability to generalise beyond their training data and have a memory capacity that scales with the number of their trainable parameters.

Previous work has touched on the topic of rendering discrete data structures such as stacks continuous, especially within the context of modelling pushdown automata with neural networks [10, 11, 3, 12]. We were inspired by the continuous pop and push operations of these architectures and the idea of an RNN controlling the data structure when developing our own models. The key difference is that our work adapts these operations to work within a recurrent continuous Stack/Queue/DeQue-like structure, the dynamics of which are fully decoupled from those of the RNN controlling it. In our models, the backwards dynamics are easily analysable in order to obtain the exact partial derivatives for use in error propagation, rather than having to approximate them as done in previous work.

In a parallel effort to ours, researchers are exploring the addition of memory to recurrent networks. The NTM and Memory Networks [4, 13, 14] provide powerful random access memory operations, whereas we focus on a more efficient and restricted class of models which we believe are sufficient for natural language transduction tasks. More closely related to our work, [15] have sought to develop a continuous stack controlled by an RNN. Note that this model—unlike the work proposed here—renders discrete push and pop operations continuous by “mixing” information across levels of the stack at each time step according to scalar push/pop action values. This means the model ends up compressing information in the stack, thereby limiting its use, as it effectively loses the unbounded memory nature of traditional symbolic models.

3 Models

In this section, we present an extensible memory enhancement to recurrent layers which can be set up to act as a continuous version of a classical Stack, Queue, or DeQue (double-ended queue). We begin by describing the operations and dynamics of a neural Stack, before showing how to modify it to act as a Queue, and extend it to act as a DeQue.

3.1 Neural Stack

Let a Neural Stack be a differentiable structure onto and from which continuous vectors are pushed and popped. Inspired by the neural pushdown automaton of [3], we render these traditionally discrete operations continuous by letting push and pop operations be real values in the interval $(0, 1)$. Intuitively, we can interpret these values as the *degree of certainty* with which some controller wishes to push a vector v onto the stack, or pop the top of the stack.

$$V_t[i] = \begin{cases} V_{t-1}[i] & \text{if } 1 \leq i < t \\ \mathbf{v}_t & \text{if } i = t \end{cases} \quad (\text{Note that } V_t[i] = \mathbf{v}_i \text{ for all } i \leq t) \quad (1)$$

$$\mathbf{s}_t[i] = \begin{cases} \max(0, \mathbf{s}_{t-1}[i] - \max(0, u_t - \sum_{j=i+1}^{t-1} \mathbf{s}_{t-1}[j])) & \text{if } 1 \leq i < t \\ d_t & \text{if } i = t \end{cases} \quad (2)$$

$$\mathbf{r}_t = \sum_{i=1}^t (\min(\mathbf{s}_t[i], \max(0, 1 - \sum_{j=i+1}^t \mathbf{s}_t[j]))) \cdot V_t[i] \quad (3)$$

Formally, a Neural Stack, fully parametrised by an embedding size m , is described at some timestep t by a $t \times m$ value matrix V_t and a strength vector $\mathbf{s}_t \in \mathbb{R}^t$. These form the core of a recurrent layer which is acted upon by a controller by receiving, from the controller, a value $\mathbf{v}_t \in \mathbb{R}^m$, a pop signal $u_t \in (0, 1)$, and a push signal $d_t \in (0, 1)$. It outputs a read vector $\mathbf{r}_t \in \mathbb{R}^m$. The recurrence of this layer comes from the fact that it will receive as previous state of the stack the pair $(V_{t-1}, \mathbf{s}_{t-1})$, and produce as next state the pair (V_t, \mathbf{s}_t) following the dynamics described below. Here, $V_t[i]$ represents the i th row (an m -dimensional vector) of V_t and $\mathbf{s}_t[i]$ represents the i th value of \mathbf{s}_t .

Equation 1 shows the update of the value component of the recurrent layer state represented as a matrix, the number of rows of which grows with time, maintaining a record of the values pushed to the stack at each timestep (whether or not they are still logically on the stack). Values are appended to the bottom of the matrix (top of the stack) and never changed.

Equation 2 shows the effect of the push and pop signal in updating the strength vector \mathbf{s}_{t-1} to produce \mathbf{s}_t . First, the pop operation removes objects from the stack. We can think of the pop value u_t as the initial deletion quantity for the operation. We traverse the strength vector \mathbf{s}_{t-1} from the highest index to the lowest. If the next strength scalar is less than the remaining deletion quantity, it is subtracted from the remaining quantity and its value is set to 0. If the remaining deletion quantity is less than the next strength scalar, the remaining deletion quantity is subtracted from that scalar and deletion stops. Next, the push value is set as the strength for the value added in the current timestep.

Equation 3 shows the dynamics of the read operation, which are similar to the pop operation. A fixed initial read quantity of 1 is set at the top of a temporary copy of the strength vector \mathbf{s}_t which is traversed from the highest index to the lowest. If the next strength scalar is smaller than the remaining read quantity, its value is preserved for this operation and subtracted from the remaining read quantity. If not, it is temporarily set to the remaining read quantity, and the strength scalars of all lower indices are temporarily set to 0. The output \mathbf{r}_t of the read operation is the weighted sum of the rows of V_t , scaled by the temporary scalar values created during the traversal. An example of the stack read calculations across three timesteps, after pushes and pops as described above, is illustrated in Figure 1a. The third step shows how setting the strength $\mathbf{s}_3[2]$ to 0 for $V_3[2]$ logically removes \mathbf{v}_2 from the stack, and how it is ignored during the read.

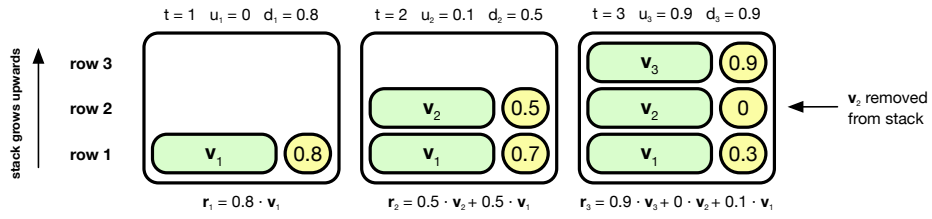
This completes the description of the forward dynamics of a neural Stack, cast as a recurrent layer, as illustrated in Figure 1b. All operations described in this section are differentiable¹. The equations describing the backwards dynamics are provided in Appendix A of the supplementary materials.

3.2 Neural Queue

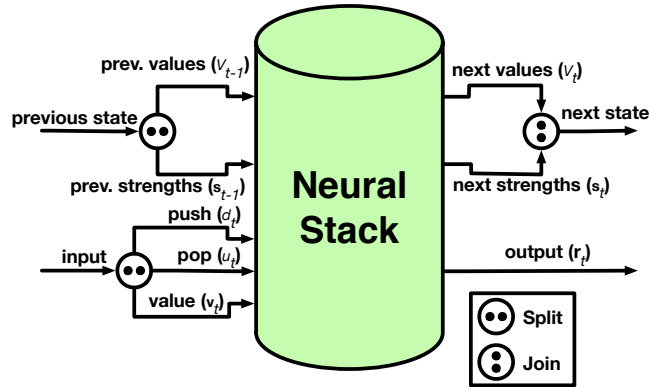
A neural Queue operates the same way as a neural Stack, with the exception that the pop operation reads the lowest index of the strength vector \mathbf{s}_t , rather than the highest. This represents popping and reading from the front of the Queue rather than the top of the stack. These operations are described in Equations 4–5.

$$\mathbf{s}_t[i] = \begin{cases} \max(0, \mathbf{s}_{t-1}[i] - \max(0, u_t - \sum_{j=1}^{i-1} \mathbf{s}_{t-1}[j])) & \text{if } 1 \leq i < t \\ d_t & \text{if } i = t \end{cases} \quad (4)$$

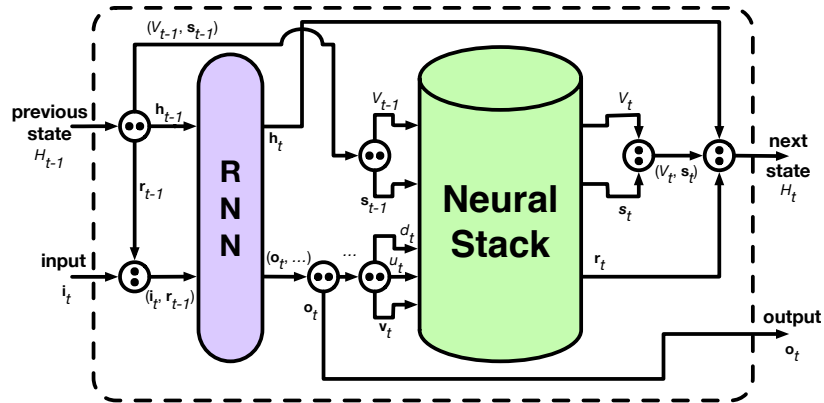
¹The $\max(x, y)$ and $\min(x, y)$ functions are technically not differentiable for $x = y$. Following the work on rectified linear units [16], we arbitrarily take the partial differentiation of the left argument in these cases.



(a) Example Operation of a Continuous Neural Stack



(b) Neural Stack as a Recurrent Layer



(c) RNN Controlling a Stack

Figure 1: Illustrating a Neural Stack's Operations, Recurrent Structure, and Control

$$\mathbf{r}_t = \sum_{i=1}^t (\min(\mathbf{s}_t[i], \max(0, 1 - \sum_{j=1}^{i-1} \mathbf{s}_t[j]))) \cdot V_t[i] \quad (5)$$

3.3 Neural DeQue

A neural DeQue operates like a neural Stack, except it takes a push, pop, and value as input for both “ends” of the structure (which we call *top* and *bot*), and outputs a read for both ends. We write u_t^{top} and u_t^{bot} instead of u_t , \mathbf{v}_t^{top} and \mathbf{v}_t^{bot} instead of \mathbf{v}_t , and so on. The state, V_t and \mathbf{s}_t are now a $2t \times m$ -dimensional matrix and a $2t$ -dimensional vector, respectively. At each timestep, a pop from the top is followed by a pop from the bottom of the DeQue, followed by the pushes and reads. The dynamics of a DeQue, which unlike a neural Stack or Queue “grows” in two directions, are described in Equations 6–11, below. Equations 7–9 decompose the strength vector update into three steps purely for notational clarity.

$$V_t[i] = \begin{cases} \mathbf{v}_t^{bot} & \text{if } i = 1 \\ \mathbf{v}_t^{top} & \text{if } i = 2t \\ V_{t-1}[i-1] & \text{if } 1 < i < 2t \end{cases} \quad (6)$$

$$\mathbf{s}_t^{top}[i] = \max(0, \mathbf{s}_{t-1}[i] - \max(0, u_t^{top} - \sum_{j=i+1}^{2(t-1)-1} \mathbf{s}_{t-1}[j])) \quad \text{if } 1 \leq i < 2(t-1) \quad (7)$$

$$\mathbf{s}_t^{both}[i] = \max(0, \mathbf{s}_t^{top}[i] - \max(0, u_t^{bot} - \sum_{j=1}^{i-1} \mathbf{s}_t^{top}[j])) \quad \text{if } 1 \leq i < 2(t-1) \quad (8)$$

$$\mathbf{s}_t[i] = \begin{cases} \mathbf{s}_t^{both}[i-1] & \text{if } 1 < i < 2t \\ d_t^{bot} & \text{if } i = 1 \\ d_t^{top} & \text{if } i = 2t \end{cases} \quad (9)$$

$$\mathbf{r}_t^{top} = \sum_{i=1}^{2t} (\min(\mathbf{s}_t[i], \max(0, 1 - \sum_{j=i+1}^{2t} \mathbf{s}_t[j]))) \cdot V_t[i] \quad (10)$$

$$\mathbf{r}_t^{bot} = \sum_{i=1}^{2t} (\min(\mathbf{s}_t[i], \max(0, 1 - \sum_{j=1}^{i-1} \mathbf{s}_t[j]))) \cdot V_t[i] \quad (11)$$

To summarise, a neural DeQue acts like two neural Stacks operated on in tandem, except that the pushes and pops from one end may eventually affect pops and reads on the other, and vice versa.

3.4 Interaction with a Controller

While the three memory modules described can be seen as recurrent layers, with the operations being used to produce the next state and output from the input and previous state being fully differentiable, they contain no tunable parameters to optimise during training. As such, they need to be attached to a controller in order to be used for any practical purposes. In exchange, they offer an extensible memory, the logical size of which is unbounded and decoupled from both the nature and parameters of the controller, and from the size of the problem they are applied to. Here, we describe how any RNN controller may be enhanced by a neural Stack, Queue or DeQue.

We begin by giving the case where the memory is a neural Stack, as illustrated in Figure 1c. Here we wish to replicate the overall ‘interface’ of a recurrent layer—as seen from outside the dotted lines—which takes the previous recurrent state H_{t-1} and an input vector \mathbf{i}_t , and transforms them to return the next recurrent state H_t and an output vector \mathbf{o}_t . In our setup, the previous state H_{t-1} of the recurrent layer will be the tuple $(\mathbf{h}_{t-1}, \mathbf{r}_{t-1}, (V_{t-1}, \mathbf{s}_{t-1}))$, where \mathbf{h}_{t-1} is the previous state of the RNN, \mathbf{r}_{t-1} is the previous stack read, and $(V_{t-1}, \mathbf{s}_{t-1})$ is the previous state of the stack as described above. With the exception of \mathbf{h}_0 , which is initialised randomly and optimised during training, all other initial states, \mathbf{r}_0 and (V_0, \mathbf{s}_0) , are set to 0-valued vectors/matrices and not updated during training.

The overall input \mathbf{i}_t is concatenated with previous read \mathbf{r}_{t-1} and passed to the RNN controller as input along with the previous controller state \mathbf{h}_{t-1} . The controller outputs its next state \mathbf{h}_t and a controller output \mathbf{o}'_t , from which we obtain the push and pop scalars d_t and u_t and the value vector \mathbf{v}_t , which are passed to the stack, as well as the network output \mathbf{o}_t :

$$\begin{aligned} d_t &= \text{sigmoid}(W_d \mathbf{o}'_t + b_d) & u_t &= \text{sigmoid}(W_u \mathbf{o}'_t + b_u) \\ \mathbf{v}_t &= \text{tanh}(W_v \mathbf{o}'_t + \mathbf{b}_v) & \mathbf{o}_t &= \text{tanh}(W_o \mathbf{o}'_t + \mathbf{b}_o) \end{aligned}$$

where W_d and W_u are vector-to-scalar projection matrices, and b_d and b_u are their scalar biases; W_v and W_o are vector-to-vector projections, and \mathbf{b}_d and \mathbf{b}_u are their vector biases, all randomly initialised and then tuned during training. Along with the previous stack state $(V_{t-1}, \mathbf{s}_{t-1})$, the stack operations d_t and u_t and the value \mathbf{v}_t are passed to the neural stack to obtain the next read \mathbf{r}_t and next stack state (V_t, \mathbf{s}_t) , which are packed into a tuple with the controller state \mathbf{h}_t to form the next state H_t of the overall recurrent layer. The output vector \mathbf{o}_t serves as the overall output of the recurrent layer. The structure described here can be adapted to control a neural Queue instead of a stack by substituting one memory module for the other.

The only additional trainable parameters in either configuration, relative to a non-enhanced RNN, are the projections for the input concatenated with the previous read into the RNN controller, and the projections from the controller output into the various Stack/Queue inputs, described above. In the case of a DeQue, both the top read \mathbf{r}^{top} and bottom read \mathbf{r}^{bot} must be preserved in the overall state. They are both concatenated with the input to form the input to the RNN controller. The output of the controller must have additional projections to output push/pop operations and values for the bottom of the DeQue. This roughly doubles the number of additional tunable parameters “wrapping” the RNN controller, compared to the Stack/Queue case.

4 Experiments

In every experiment, integer-encoded source and target sequence pairs are presented to the candidate model as a batch of single joint sequences. The joint sequence starts with a start-of-sequence (SOS) symbol, and ends with an end-of-sequence (EOS) symbol, with a separator symbol separating the source and target sequences. Integer-encoded symbols are converted to 64-dimensional embeddings via an embedding matrix, which is randomly initialised and tuned during training. Separate word-to-index mappings are used for source and target vocabularies. Separate embedding matrices are used to encode input and output (predicted) embeddings.

4.1 Synthetic Transduction Tasks

The aim of each of the following tasks is to read an input sequence, and generate as target sequence a transformed version of the source sequence, followed by an EOS symbol. Source sequences are randomly generated from a vocabulary of 128 meaningless symbols. The length of each training source sequence is uniformly sampled from $\text{unif}\{8, 64\}$, and each symbol in the sequence is drawn with replacement from a uniform distribution over the source vocabulary (ignoring SOS, and separator).

A deterministic task-specific transformation, described for each task below, is applied to the source sequence to yield the target sequence. As the training sequences are entirely determined by the source sequence, there are close to 10^{135} training sequences for each task, and training examples are sampled from this space due to the random generation of source sequences. The following steps are followed before each training and test sequence are presented to the models, the SOS symbol ($\langle s \rangle$) is prepended to the source sequence, which is concatenated with a separator symbol ($|||$) and the target sequences, to which the EOS symbol ($\langle /s \rangle$) is appended.

Sequence Copying The source sequence is copied to form the target sequence. Sequences have the form:

$$\langle s \rangle a_1 \dots a_k ||| a_1 \dots a_k \langle /s \rangle$$

Sequence Reversal The source sequence is deterministically reversed to produce the target sequence. Sequences have the form:

$$\langle s \rangle a_1 a_2 \dots a_k ||| a_k \dots a_2 a_1 \langle /s \rangle$$

Bigram flipping The source side is restricted to even-length sequences. The target is produced by swapping, for all odd source sequence indices $i \in [1, |seq|] \wedge \text{odd}(i)$, the i th symbol with the $(i + 1)$ th symbol. Sequences have the form:

$$\langle s \rangle a_1 a_2 a_3 a_4 \dots a_{k-1} a_k ||| a_2 a_1 a_4 a_3 \dots a_k a_{k-1} \langle /s \rangle$$

4.2 ITG Transduction Tasks

The following tasks examine how well models can approach sequence transduction problems where the source and target sequence are jointly generated by Inversion Transduction Grammars (ITG) [8], a subclass of Synchronous Context-Free Grammars [17] often used in machine translation [18]. We present two simple ITG-based datasets with interesting linguistic properties and their underlying grammars. We show these grammars in Table 1, in Appendix C of the supplementary materials. For each synchronised non-terminal, an expansion is chosen according to the probability distribution specified by the rule probability p at the beginning of each rule. For each grammar, ‘A’ is always the root of the ITG tree.

We tuned the generative probabilities for recursive rules by hand so that the grammars generate left and right sequences of lengths 8 to 128 with relatively uniform distribution. We generate training data by rejecting samples that are outside of the range [8, 64], and testing data by rejecting samples outside of the range [65, 128]. For terminal symbol-generating rules, we balance the classes so that for k terminal-generating symbols in the grammar, each terminal-generating non-terminal ‘X’ generates a vocabulary of approximately $128/k$, and each vocabulary word under that class is equiprobable. These design choices were made to maximise the similarity between the experimental settings of the ITG tasks described here and the synthetic tasks described above.

Subj–Verb–Obj to Subj–Obj–Verb A persistent challenge in machine translation is to learn to faithfully reproduce high-level syntactic divergences between languages. For instance, when translating an English sentence with a non-finite verb into German, a transducer must locate and move the verb over the object to the final position. We simulate this phenomena with a synchronous grammar which generates strings exhibiting verb movements. To add an extra challenge, we also simulate simple relative clause embeddings to test the models’ ability to transduce in the presence of unbounded recursive structures.

A sample output of the grammar is presented here, with spaces between words being included for stylistic purposes, and where s, o, and v indicate subject, object, and verb terminals respectively, i and o mark input and output, and rp indicates a relative pronoun:

si1 vi28 oi5 oi7 si15 rpi si19 vi16 oi10 oi24 ||| so1 oo5 oo7 so15 rpo so19 vo16 oo10 oo24 vo28

Genderless to gendered grammar We design a small grammar to simulate translations from a language with gender-free articles to one with gender-specific definite and indefinite articles. A real world example of such a translation would be from English (*the, a*) to German (*der/die/das, ein/eine/ein*).

The grammar simulates sentences in $(NP/(V/NP))$ or (NP/V) form, where every noun phrase can become an infinite sequence of nouns joined by a conjunction. Each noun in the source language has a neutral definite or indefinite article. The matching word in the target language then needs to be preceded by its appropriate article. A sample output of the grammar is presented here, with spaces between words being included for stylistic purposes:

we11 the en19 and the em17 ||| wg11 das gn19 und der gm17

4.3 Evaluation

For each task, test data is generated through the same procedure as training data, with the key difference that the length of the source sequence is sampled from $\text{unif}\{65, 128\}$. As a result of this change, we not only are assured that the models cannot observe any test sequences during training, but are also measuring how well the sequence transduction capabilities of the evaluated models generalise beyond the sequence lengths observed during training. To control for generalisation ability, we also report accuracy scores on sequences separately sampled from the training set, which given the size of the sample space are unlikely to have ever been observed during actual model training.

For each round of testing, we sample 1000 sequences from the appropriate test set. For each sequence, the model reads in the source sequence and separator symbol, and begins generating the next symbol by taking the maximally likely symbol from the softmax distribution over target symbols produced by the model at each step. Based on this process, we give each model a *coarse accuracy* score, corresponding to the proportion of test sequences correctly predicted from beginning until end (EOS symbol) without error, as well as a *fine accuracy* score, corresponding to the average proportion of each sequence correctly generated before the first error. Formally, we have:

$$coarse = \frac{\#correct}{\#seqs} \quad fine = \frac{1}{\#seqs} \sum_{i=1}^{\#seqs} \frac{\#correct_i}{|target_i|}$$

where $\#correct$ and $\#seqs$ are the number of correctly predicted sequences (end-to-end) and the total number of sequences in the test batch (1000 in this experiment), respectively; $\#correct_i$ is the number of correctly predicted symbols before the first error in the i th sequence of the test batch, and $|target_i|$ is the length of the target segment that sequence (including EOS symbol).

4.4 Models Compared and Experimental Setup

For each task, we use as benchmarks the Deep LSTMs described in [1], with 1, 2, 4, and 8 layers. Against these benchmarks, we evaluate neural Stack-, Queue-, and DeQue-enhanced LSTMs. When running experiments, we trained and tested a version of each model where all LSTMs in each model have a hidden layer size of 256, and one for a hidden layer size of 512. The Stack/Queue/DeQue embedding size was arbitrarily set to 256, half the maximum hidden size. The number of parameters for each model are reported for each architecture in Table 2 of the appendix. Concretely, the neural Stack-, Queue-, and DeQue-enhanced LSTMs have the same number of trainable parameters as a two-layer Deep LSTM. These all come from the extra connections to and from the memory module, which itself has no trainable parameters, regardless of its logical size.

Models are trained with minibatch RMSProp [19], with a batch size of 10. We grid-searched learning rates across the set $\{5 \times 10^{-3}, 1 \times 10^{-3}, 5 \times 10^{-4}, 1 \times 10^{-4}, 5 \times 10^{-5}\}$. We used gradient clipping [20], clipping all gradients above 1. Average training perplexity was calculated every 100 batches. Training and test set accuracies were recorded every 1000 batches.

5 Results and Discussion

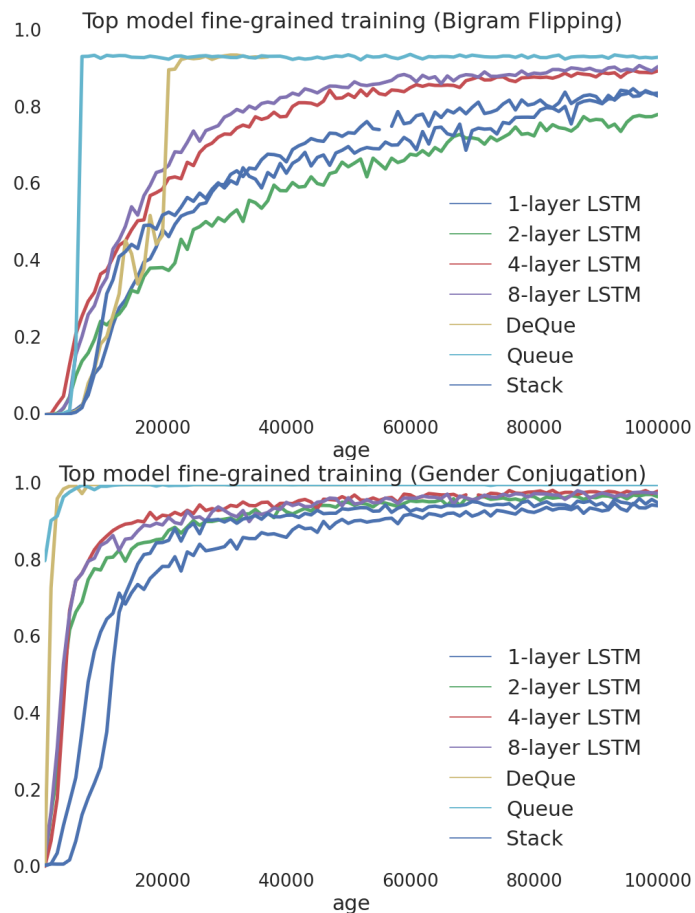
Because of the impossibility of overfitting the datasets, we let the models train an unbounded number of steps, and report results at convergence. We present in Figure 2a the coarse- and fine-grained accuracies, for each task, of the best model of each architecture described in this paper alongside the best performing Deep LSTM benchmark. The best models were automatically selected based on average training perplexity. The LSTM benchmarks performed similarly across the range of random initialisations, so the effect of this procedure is primarily to try and select the better performing Stack/Queue/DeQue-enhanced LSTM. In most cases, this procedure does not yield the actual best-performing model, and in practice a more sophisticated procedure such as ensembling [21] should produce better results.

For all experiments, the Neural Stack or Queue outperforms the Deep LSTM benchmarks, often by a significant margin. For most experiments, if a Neural Stack- or Queue-enhanced LSTM learns to partially or consistently solve the problem, then so does the Neural DeQue. For experiments where the enhanced LSTMs solve the problem completely (consistent accuracy of 1) in training, the accuracy persists in longer sequences in the test set, whereas benchmark accuracies drop for all experiments except the SVO to SOV and Gender Conjugation ITG transduction tasks. Across all tasks which the enhanced LSTMs solve, the convergence on the top accuracy happens orders of magnitude earlier for enhanced LSTMs than for benchmark LSTMs, as exemplified in Figure 2b.

The results for the sequence inversion and copying tasks serve as unit tests for our models, as the controller mainly needs to learn to push the appropriate number of times and then pop continuously. Nonetheless, the failure of Deep LSTMs to learn such a regular pattern and generalise is itself indicative of the limitations of the benchmarks presented here, and of the relative expressive power of our models. Their ability to generalise perfectly to sequences up to twice as long as those attested during training is also notable, and also attested in the other experiments. Finally, this pair of

Experiment	Model	Training		Testing	
		Coarse	Fine	Coarse	Fine
Sequence Copying	4-layer LSTM	0.98	0.98	0.01	0.50
	Stack-LSTM	0.89	0.94	0.00	0.22
	Queue-LSTM	1.00	1.00	1.00	1.00
	DeQue-LSTM	1.00	1.00	1.00	1.00
Sequence Reversal	8-layer LSTM	0.95	0.98	0.04	0.13
	Stack-LSTM	1.00	1.00	1.00	1.00
	Queue-LSTM	0.44	0.61	0.00	0.01
	DeQue-LSTM	1.00	1.00	1.00	1.00
Bigram Flipping	2-layer LSTM	0.54	0.93	0.02	0.52
	Stack-LSTM	0.44	0.90	0.00	0.48
	Queue-LSTM	0.55	0.94	0.55	0.98
	DeQue-LSTM	0.55	0.94	0.53	0.98
SVO to SOV	8-layer LSTM	0.98	0.99	0.98	0.99
	Stack-LSTM	1.00	1.00	1.00	1.00
	Queue-LSTM	1.00	1.00	1.00	1.00
	DeQue-LSTM	1.00	1.00	1.00	1.00
Gender Conjugation	8-layer LSTM	0.98	0.99	0.99	0.99
	Stack-LSTM	0.93	0.97	0.93	0.97
	Queue-LSTM	1.00	1.00	1.00	1.00
	DeQue-LSTM	1.00	1.00	1.00	1.00

(a) Comparing Enhanced LSTMs to Best Benchmarks



(b) Comparison of Model Convergence during Training

Figure 2: Results on the transduction tasks and convergence properties

experiments illustrates how while the neural Queue solves copying and the Stack solves reversal, a simple LSTM controller can learn to operate a DeQue as either structure, and solve both tasks.

The results of the Bigram Flipping task for all models are consistent with the failure to consistently correctly generate the last two symbols of the sequence. We hypothesise that both Deep LSTMs and our models economically learn to pairwise flip the sequence tokens, and attempt to do so half the time when reaching the EOS token. For the two ITG tasks, the success of Deep LSTM benchmarks relative to their performance in other tasks can be explained by their ability to exploit short local dependencies dominating the longer dependencies in these particular grammars.

Overall, the rapid convergence, where possible, on a general solution to a transduction problem in a manner which propagates to longer sequences without loss of accuracy is indicative that an unbounded memory-enhanced controller can learn to solve these problems procedurally, rather than memorising the underlying distribution of the data.

6 Conclusions

The experiments performed in this paper demonstrate that single-layer LSTMs enhanced by an unbounded differentiable memory capable of acting, in the limit, like a classical Stack, Queue, or DeQue, are capable of solving sequence-to-sequence transduction tasks for which Deep LSTMs falter. Even in tasks for which benchmarks obtain high accuracies, the memory-enhanced LSTMs converge earlier, and to higher accuracies, while requiring considerably fewer parameters than all but the simplest of Deep LSTMs. We therefore believe these constitute a crucial addition to our neural network toolbox, and that more complex linguistic transduction tasks such as machine translation or parsing will be rendered more tractable by their inclusion.

Acknowledgements We thank Alex Graves, Demis Hassabis, Tomáš Kočiský, Tim Rocktäschel, Sam Ritter, Geoff Hinton, Ilya Sutskever, Chris Dyer, and many others for their helpful comments.

References

- [1] Ilya Sutskever, Oriol Vinyals, and Quoc V. V Le. Sequence to sequence learning with neural networks. In Z. Ghahramani, M. Welling, C. Cortes, N.D. Lawrence, and K.Q. Weinberger, editors, *Advances in Neural Information Processing Systems 27*, pages 3104–3112. Curran Associates, Inc., 2014.
- [2] Kyunghyun Cho, Bart van Merriënboer, Caglar Gulcehre, Fethi Bougares, Holger Schwenk, and Yoshua Bengio. Learning phrase representations using rnn encoder-decoder for statistical machine translation. *arXiv preprint arXiv:1406.1078*, 2014.
- [3] GZ Sun, C Lee Giles, HH Chen, and YC Lee. The neural network pushdown automaton: Model, stack and learning simulations. 1998.
- [4] Alex Graves, Greg Wayne, and Ivo Danihelka. Neural turing machines. *CoRR*, abs/1410.5401, 2014.
- [5] Alex Graves. *Supervised Sequence Labelling with Recurrent Neural Networks*, volume 385 of *Studies in Computational Intelligence*. Springer, 2012.
- [6] Markus Dreyer, Jason R. Smith, and Jason Eisner. Latent-variable modeling of string transductions with finite-state methods. In *Proceedings of the Conference on Empirical Methods in Natural Language Processing, EMNLP '08*, pages 1080–1089, Stroudsburg, PA, USA, 2008. Association for Computational Linguistics.
- [7] Cyril Allauzen, Michael Riley, Johan Schalkwyk, Wojciech Skut, and Mehryar Mohri. OpenFST: A general and efficient weighted finite-state transducer library. In *Implementation and Application of Automata*, volume 4783 of *Lecture Notes in Computer Science*, pages 11–23. Springer Berlin Heidelberg, 2007.
- [8] Dekai Wu. Stochastic inversion transduction grammars and bilingual parsing of parallel corpora. *Computational linguistics*, 23(3):377–403, 1997.
- [9] Alex Graves. Sequence transduction with recurrent neural networks. In *Representation Learning Workshop, ICML*. 2012.
- [10] Sreerupa Das, C Lee Giles, and Guo-Zheng Sun. Learning context-free grammars: Capabilities and limitations of a recurrent neural network with an external stack memory. In *Proceedings of The Fourteenth Annual Conference of Cognitive Science Society. Indiana University*, 1992.
- [11] Sreerupa Das, C Lee Giles, and Guo-Zheng Sun. Using prior knowledge in a {NNPDA} to learn context-free languages. *Advances in neural information processing systems*, 1993.
- [12] Chris Dyer, Miguel Ballesteros, Wang Ling, Austin Matthews, and Noah A Smith. Transition-based dependency parsing with stack long short-term memory. In *Proceedings of the 53rd Annual Meeting of the Association for Computational Linguistics and the 7th International Joint Conference on Natural Language Processing (Volume 1: Long Papers)*, ACL '15, pages 334–343, Beijing, China, 2015. Association for Computational Linguistics.
- [13] Sainbayar Sukhbaatar, Arthur Szlam, Jason Weston, and Rob Fergus. Weakly supervised memory networks. *CoRR*, abs/1503.08895, 2015.
- [14] Wojciech Zaremba and Ilya Sutskever. Reinforcement learning neural turing machines. *arXiv preprint arXiv:1505.00521*, 2015.
- [15] Armand Joulin and Tomas Mikolov. Inferring algorithmic patterns with stack-augmented recurrent nets. *arXiv preprint arXiv:1503.01007*, 2015.
- [16] Vinod Nair and Geoffrey E Hinton. Rectified linear units improve restricted boltzmann machines. In *Proceedings of the 27th International Conference on Machine Learning (ICML-10)*, pages 807–814, 2010.
- [17] Alfred V Aho and Jeffrey D Ullman. *The theory of parsing, translation, and compiling*. Prentice-Hall, Inc., 1972.
- [18] Dekai Wu and Hongsing Wong. Machine translation with a stochastic grammatical channel. In *Proceedings of the 17th international conference on Computational linguistics-Volume 2*, pages 1408–1415. Association for Computational Linguistics, 1998.
- [19] Tijmen Tieleman and Geoffrey Hinton. Lecture 6.5-rmsprop: Divide the gradient by a running average of its recent magnitude. *COURSERA: Neural Networks for Machine Learning*, 4, 2012.
- [20] Razvan Pascanu, Tomas Mikolov, and Yoshua Bengio. Understanding the exploding gradient problem. *Computing Research Repository (CoRR) abs/1211.5063*, 2012.
- [21] Zhi-Hua Zhou, Jianxin Wu, and Wei Tang. Ensembling neural networks: many could be better than all. *Artificial intelligence*, 137(1):239–263, 2002.

A Analysis of the Backwards Dynamics of a Neural Stack

We describe here the backwards dynamics of the neural stack by examining the relevant partial derivatives of the outputs with regard to the inputs, as defined in Equations 1–3. We use δ_{ij} to indicate the Kronecker delta (1 if $i = j$, 0 otherwise). The equations below hold for any valid row numbers i and n .

$$\frac{\partial V_t[i]}{\partial V_{t-1}[n]} = \delta_{in} \quad (12) \quad \frac{\partial V_t[i]}{\partial \mathbf{v}_t} = \delta_{it} \quad (13) \quad \frac{\partial \mathbf{s}_t[i]}{\partial d_t} = \delta_{it} \quad (14)$$

$$\frac{\partial \mathbf{r}_t}{\partial V_t[n]} = \min(\mathbf{s}_t[n], \max(0, 1 - \sum_{j=n+1}^t \mathbf{s}_t[j])) \quad \text{and} \quad \frac{\partial \mathbf{r}_t}{\partial \mathbf{v}_t} = \frac{\partial \mathbf{r}_t}{\partial V_t[t]} = d_t \quad (15)$$

$$\frac{\partial \mathbf{s}_t[i]}{\partial \mathbf{s}_{t-1}[n]} = \begin{cases} 1 & \text{if } i < n < t \text{ and } \mathbf{s}_t[i] > 0 \text{ and } u_t - \sum_{j=i+1}^{t-1} \mathbf{s}_{t-1}[j] > 0 \\ \delta_{in} & \text{if } i < t \text{ and } \mathbf{s}_t[i] > 0 \text{ and } u_t - \sum_{j=i+1}^{t-1} \mathbf{s}_{t-1}[j] \leq 0 \\ 0 & \text{otherwise} \end{cases} \quad (16)$$

$$\frac{\partial \mathbf{s}_t[i]}{\partial u_t} = \begin{cases} -1 & \text{if } i < t \text{ and } \mathbf{s}_t[i] > 0 \text{ and } u_t - \sum_{j=i+1}^{t-1} \mathbf{s}_{t-1}[j] > 0 \\ 0 & \text{otherwise} \end{cases} \quad (17)$$

$$\frac{\partial \mathbf{r}_t}{\partial \mathbf{s}_t[n]} = \sum_{i=1}^t h(i, n) \cdot V_t[i] \quad (18)$$

$$\text{where } h(i, n) = \begin{cases} \delta_{in} & \text{if } \mathbf{s}_t[i] \leq \max(0, 1 - \sum_{j=i+1}^t \mathbf{s}_t[j]) \\ -1 & \text{if } i < n \text{ and } \mathbf{s}_t[i] > \max(0, 1 - \sum_{j=i+1}^t \mathbf{s}_t[j]) \\ & \text{and } \sum_{j=i+1}^t \mathbf{s}_t[j] \leq 1 \\ 0 & \text{otherwise} \end{cases}$$

All partial derivatives other than those obtained by the chain rule for derivatives can be assumed to be 0. The backwards dynamics for neural Queues and DeQueues can be similarly derived from Equations 4–11.

B A Note on Controller Initialisation

During initial experiments with the continuous stack presented in this paper, we noted that the stack’s ability to learn the solution to the transduction tasks detailed here varied greatly based on the random initialisation of the controller. This initially required us to restart training with different random seeds to obtain behaviour consistent with the learning of an algorithmic solution (i.e. rapid drop in validation perplexity after a short number of iterations).

Analysis of the backwards dynamics presented in Section A demonstrates that error on push and pop decisions is a function of read error “carried” back through time by the vectors on the stack (*cf.* Equation 14 and Equations 17–18), which is accumulated as the vectors placed onto the stack by a push, or retained after a pop, are read at further timesteps. Crucially, this means that if the controller operating the stack is initially biased in favour of popping over pushing (i.e. $u_{t+1} > d_t$ for most or all timesteps t), vectors are likely to be removed from the stack the timestep after they were pushed, resulting in the continuous stack being used as an extra recurrent hidden layer, rather than as something behaving like a classical stack.

The consequence of this is that gradient for the decision to push at time t only comes via the hidden state of the controller at time $t + 1$, so for problems where the vector would ideally have been

preserved on the stack until some later time, signal encouraging the controller to push with higher certainty is unlikely to be propagated back if the RNN controller suffers from vanishing gradient issues. Likewise, the gradient for the decision to pop is 0 (as each pop empties the stack). We conclude that under-using the memory in such a way makes its proper manipulation hard to learn by the controller.

Conversely, over-using the stack (even incorrectly) means that gradient obtained with regard to the (mis)use is properly communicated, as the pop gradient will not be zero (Equation 17) for all t . Additionally, the (non-vanishing) gradient propagated through the stack state (Equation 12) will allow the decision to push at some timestep to be rewarded or penalised based on reads at some much later time. These remarks also apply to the continuous queue and double-ended queue.

Since in our setting the decision to push and pop is produced by taking a biased linear transform of an RNN hidden state followed by a component-wise sigmoid operation, we hypothesised, based on the above analysis, that initialising the bias for popping to a negative number would solve the variance issue described above. We tested this on short sequences of the copy task, and found that a small bias of -1 produced the desired algorithmic behaviour of the stack-enhanced controller across all seeds tested. Setting this initialisation policy for the controller across all experiments allowed us to reproduce the results produced in the paper without need for repeated initialisation. We recommend that other controller implementations provide similar trainable biases for the decision to pop, and initialise them following this policy (and likewise for controllers controlling other continuous data structures presented in this paper).

C Inversion Transduction Grammars used in Experiments

We present here, in Table 1, the inverse transduction grammars described in Section 4.2. Sets of terminal-generating rules are indicated by the form ‘ $X_i \rightarrow \dots$ ’, where $i \in [1, k]$ and $p(X_i) \approx (100/k)^{-1}$ for k terminal generating non-terminal symbols (classes of terminals), so that the generated vocabulary is balanced across classes and of a size similar to other experiments.

p	ITG Rules	p	ITG Rules
1	$A \rightarrow S1\ VT2\ O3 \mid S1\ O3\ VT2$	1	$A \rightarrow B1 \mid B1$
1/5	$S \rightarrow S1\ S2 \mid S1\ S2$	1/4	$B \rightarrow B1\ \text{or}\ B2 \mid B1\ \text{oder}\ B2$
1/5	$S \rightarrow S1\ rpi\ S2\ VT3 \mid S1\ rpo\ S2\ VT3$	1/4	$B \rightarrow S1\ \text{and}\ S2 \mid S1\ \text{und}\ S2$
3/5	$S \rightarrow ST1 \mid ST1$	1/2	$B \rightarrow B1\ V1 \mid B1\ V1$
1/5	$O \rightarrow O1\ O2 \mid O1\ O2$	3/4	$V \rightarrow W1\ B2 \mid W1\ B2$
1/5	$O \rightarrow S1\ rpi\ S2\ VT3 \mid S1\ rpo\ S2\ VT3$	1/4	$V \rightarrow W1 \mid W1$
3/5	$O \rightarrow OT1 \mid OT1$	1/6	$S \rightarrow \text{the}\ M1 \mid \text{der}\ M1$
1/33	$ST_i \rightarrow si_i \mid so_i$	1/6	$S \rightarrow \text{the}\ F1 \mid \text{die}\ F1$
1/33	$OT_i \rightarrow oi_i \mid oo_i$	1/6	$S \rightarrow \text{the}\ N1 \mid \text{das}\ N1$
1/33	$VT_i \rightarrow vi_i \mid vo_i$	1/6	$S \rightarrow a\ M1 \mid \text{ein}\ M1$
	(a) SVO-SOV Grammar	1/6	$S \rightarrow a\ F1 \mid \text{eine}\ F1$
		1/6	$S \rightarrow a\ N1 \mid \text{ein}\ N1$
		1/25	$W_i \rightarrow we_i \mid wg_i$
		1/25	$M_i \rightarrow me_i \mid mg_i$
		1/25	$F_i \rightarrow fe_i \mid fg_i$
		1/25	$N_i \rightarrow ne_i \mid ng_i$
			(b) English-German Conjugation Grammar

Table 1: Inversion Transduction Grammars used in ITG Tasks

D Model Sizes

We show, in Table 2, the number of parameters per model, for all models used in the experiments of the paper.

Model	Hidden layer size	
	256	512
1-layer LSTM	3.3×10^5	1.2×10^6
2-layer LSTM	9.1×10^5	3.4×10^6
4-layer LSTM	2.1×10^6	7.8×10^6
8-layer LSTM	4.5×10^6	1.7×10^7
Stack-LSTM	6.7×10^5	1.9×10^6
Queue-LSTM	6.7×10^5	1.9×10^6
DeQue-LSTM	1.0×10^6	2.5×10^6

Table 2: Number of trainable parameters per model

E Full Results

We show in Table 3 the full results for each task of the best performing models. The procedure for selecting the best performing model is described in Section 5.

Experiment	Model	Training		Testing	
		Coarse	Fine	Coarse	Fine
Sequence Copying	1-layer LSTM	0.62	0.87	0.00	0.38
	2-layer LSTM	0.80	0.95	0.00	0.47
	4-layer LSTM	0.98	0.98	0.01	0.50
	8-layer LSTM	0.57	0.83	0.00	0.31
	Stack-LSTM	0.89	0.94	0.00	0.22
	Queue-LSTM	1.00	1.00	1.00	1.00
	DeQue-LSTM	1.00	1.00	1.00	1.00
Sequence Reversal	1-layer LSTM	0.78	0.87	0.01	0.09
	2-layer LSTM	0.91	0.94	0.02	0.06
	4-layer LSTM	0.93	0.96	0.03	0.15
	8-layer LSTM	0.95	0.98	0.04	0.13
	Stack-LSTM	1.00	1.00	1.00	1.00
	Queue-LSTM	0.44	0.61	0.00	0.07
	DeQue-LSTM	1.00	1.00	1.00	1.00
Bigram Flipping	1-layer LSTM	0.53	0.93	0.01	0.53
	2-layer LSTM	0.54	0.93	0.02	0.52
	4-layer LSTM	0.52	0.93	0.01	0.56
	8-layer LSTM	0.52	0.93	0.01	0.53
	Stack-LSTM	0.44	0.90	0.00	0.48
	Queue-LSTM	0.55	0.94	0.55	0.98
	DeQue-LSTM	0.55	0.94	0.53	0.98
SVO to SOV	1-layer LSTM	0.96	0.98	0.96	0.99
	2-layer LSTM	0.97	0.99	0.96	0.99
	4-layer LSTM	0.97	0.99	0.97	0.99
	8-layer LSTM	0.98	0.99	0.98	0.99
	Stack-LSTM	1.00	1.00	1.00	1.00
	Queue-LSTM	1.00	1.00	1.00	1.00
	DeQue-LSTM	1.00	1.00	1.00	1.00
Gender Conjugation	1-layer LSTM	0.97	0.99	0.97	0.99
	2-layer LSTM	0.98	0.99	0.98	0.99
	4-layer LSTM	0.98	0.99	0.98	0.99
	8-layer LSTM	0.98	0.99	0.99	0.99
	Stack-LSTM	0.93	0.97	0.93	0.97
	Queue-LSTM	1.00	1.00	1.00	1.00
	DeQue-LSTM	1.00	1.00	1.00	1.00

Table 3: Summary of Results for Transduction Tasks